Regional atmospheric influence on the Chandler wobble

L.V. Zotov [a,b,*], C. Bizouard [c,1]

[a] Sternberg Astronomical Institute of Moscow State University, Laboratory of Gravimetry, Russia
[b] National Research University, Higher School of Economics, Russia
[c] Paris Observatory, Service de la Rotation de la Terre, SYRTE, France

Abstract

From the maps of regional contribution to atmospheric angular momentum (AAM) over the period 1948–2011 (NCEP/NCAR reanalysis data) time domain excitation in Chandler frequency band was extracted by Panteleev's filtering method. This permits us to investigate the evolution of the regional atmospheric influence on Chandler wobble. It appears that the temperate latitudes bring the strongest inputs. For pressure term they are limited to continents, and highlight the role of Europe. For the wind term they mostly result from ocean area, encompassing in particular North Atlantic. A quasi-20 year cycle is found in the regional patterns of the atmospheric excitation. The integrated AAM is finally compared with the geodetic excitation reconstructed from the observed polar motion.
© 2014 COSPAR. Published by Elsevier Ltd. All rights reserved.

1. Introduction

With an average amplitude of 0.2 arcsec Chandler wobble is the main component of the polar motion (PM). It is a resonant oscillation (Lambeck, 1980; Sidorenkov, 2009) but as the Earth is a viscous-elastic body, it should decay with a characteristic time of ~50 years in absence of excitation (Gross, 2000). The maintaining of the Chandler wobble amplitude can be explained by exchange of angular momentum between the solid Earth and the surface fluid layer composed of atmosphere and oceans (Brzezinski et al., 2002, 2012; Brzezinski and Nastula, 2002; Gross et al., 2003; Salstein, 2000). An additional input could come from hydrological processes (Liao et al., 2007; Nastula et al., 2007). A strong argument favouring the role

of the surface fluid layer is the correlation noted between Chandler wobble amplitude variation and changeability found in the integrated effective atmospheric angular momentum (EAAM) and effective oceanic angular momentum (EOAM) (Bizouard et al., 2011) from 1950. Because of the proximity with the large annual excitation, it is a more difficult task to extract time domain Chandler excitation in both fluid layer angular momentum and geodetic excitation reconstructed from PM observations. The Chandler excitation reconstruction is an inverse problem. Different methods such as singular numbers truncation or Tikhonov regularization can be used to obtain a pseudo-solution of this problem (Zotov and Panteleev, 2012). To reduce the noise influence on the solution and to select the frequency band of interest, the Panteleev corrective filter was proposed in Panteleev and Chesnokova (2011) and was applied to PM in Zotov and Bizouard (2012) and Zotov (2010). Such a filter tapers the annual and other frequency components prior to the inversion. Zotov and Bizouard (2012) not only show the good agreement between surface fluid layer excitation and geodetic one (reconstructed from

---

* Corresponding author at: Universitetski pr., 13, Moscow 119992, Russia.

E-mail addresses: tempus@sai.msu.ru (L.V. Zotov), christian.bizouard@obspm.fr (C. Bizouard).
[1] 61, Avenue de l'Observatoire, 75014 Paris, France.

PM observations) over a 20-year time interval, but also put forward a modulation in Chandler excitation, synchronous with the 18.6-year Lunar tide.

In this paper we aim at localising the atmospheric sources of Chandler excitation by filtering regional AAM inputs in the Chandler frequency band. Like in Liao et al. (2007) and Nastula and Salstein (2012) we will determine the regional contribution to EAAM in Chandler band, but after having designed a narrow-band Panteleev filter as in Zotov and Bizouard (2012). Unlike Nastula et al. (2009, 2012, 2014), we do not calculate covariances between regional contribution to EAAM and excitation. We focus our study on filtered AAM fields in Chandler frequency band and their evolution: animated maps permit to track changes of the atmospheric excitation sources and their geographical location, Hovmoeller plots are used to characterise temporal evolution over latitude and longitude bands.

2. Initial data and method of processing

The Earth's polar motion is commonly modelled by the linear Euler–Liouville equation (Munk and MacDonald, 1960; Lambeck, 1980)

$$\frac{i}{\sigma_c}\frac{dp(t)}{dt} + p(t) = \chi^{tot}(t), \tag{1}$$

where the complex Chandler angular frequency $\sigma_c = 2\pi f_c(1 + i/2Q)$ depends on real Chandler frequency f_c and quality factor Q. In the dynamical system (1) the complex PM trajectory $p = p_1 + ip_2$ forms an output, which depends on the total input excitation $\chi^{tot} = \chi_1^{tot} + i\chi_2^{tot}$. Large part of this excitation is caused by the atmosphere. It can be described by the EAAM functions $\chi = \chi_1 + i\chi_2$, which can be calculated from the meteorological observations (Brzezinski et al., 2012; Zhong et al., 2002). The χ_1 component is the projection along the x axis of the terrestrial reference frame (TRF), and χ_2 along its y axis. Each of EAAM projections has two components – pressure (mass) χ^P and wind (motion) χ^W. The first one is related to the moment of inertia changes, the second one to the changes of atmospheric momentum with respect to the solid Earth. These one-dimensional time series $\chi^{P,W}$ provided by IERS Global Geophysical Fluids Centre (http://www.iers.org/IERS/EN/DataProducts/GeophysicalFluidsData/geoFluids.html) are usually analysed and compared to the geodetic excitation.

The EAAM functions χ are obtained through integration of regional contribution $X^{P,W}(\lambda, \phi)$ all over the globe (over all the longitudes and latitudes)

$$\chi^{P,W} = \iint X^{P,W}(\lambda, \phi)d\lambda d\phi. \tag{2}$$

So, EAAM includes the sum of inputs of atmospheric variability from different regions of the globe. The fields of $X(\lambda, \phi)$ representing regional contributions to EAAM are called just AAM (without E) throughout this paper.

We used data from NCEP/NCAR reanalysis project, obtained through meteorological data processing with use of numerical weather modelling. The interpolated fields of wind and pressure all over the globe are available since 1948 with 6-h step. The data for different heights (pressure levels) can be found at http://www.esrl.noaa.gov/psd/data/gridded/data.ncep.reanalysis.html.

These data were processed and converted to AAM maps at the Center for Astro-geodynamics of Shanghai Astronomical Observatory. For every geographical point of the longitude-latitude grid the regional pressure component was calculated according to the expression

$$\begin{aligned} X^P(\lambda, \phi) &= X_1^P + iX_2^P \\ &= \frac{1.11R^4}{(C-A)g}p_s(\lambda, \phi)\sin\phi\cos^2\phi e^{i\lambda}, \end{aligned} \tag{3}$$

and the wind component – according to

$$\begin{aligned} X^W(\lambda, \phi) &= X_1^W + iX_2^W \\ &= \frac{1.57R^3}{\Omega(C-A)g}\int (u(\lambda, \phi, p)\sin\phi \\ &\quad + iv(\lambda, \phi, p))\cos\phi e^{i\lambda}dp, \end{aligned}$$

where R and Ω are mean Earth radius and angular velocity; A, C are the principal moments of inertia of the Earth; g is the gravitational acceleration; λ and ϕ are longitude and latitude at a given grid point; p_s is surface pressure; and u, v are zonal and meridional wind velocities. The pressure term was calculated by assuming the Inverted Barometer (IB) hypotheses, i.e. the pressure compensation over water by the changes of its level (Zhou et al., 2006).

The AAM field with 6 h step and $2.5° \times 2.5°$ angular resolution were obtained. Every day has 4 maps and every map has $73 \times 144 = 10,512$ longitude-latitude points. In every point we have a time series, which are filtered in the Chandler frequency band by applying the Panteleev band-pass filter (Zotov and Bizouard, 2012). The filter's impulse response is given by

$$h(t) = \frac{\omega_0}{2\sqrt{2}}e^{-\left(\frac{\omega_0|t|}{\sqrt{2}} - i2\pi f_c t\right)}\left(\cos\frac{\omega_0 t}{\sqrt{2}} + \sin\frac{\omega_0|t|}{\sqrt{2}}\right) \tag{4}$$

with the parameter $\omega_0 = 2\pi f_0$. The filter parameter (defining its width) was selected to be $f_0 = 0.04$ yr^{-1} (see below). The transfer function of the filter (4) in frequency domain is given by expression

$$L_h(f) = \frac{f_0^4}{(f - f_c)^4 + f_0^4}. \tag{5}$$

It is centred on the Chandler frequency $f_c = 0.8435$ yr^{-1} and does not change the phase of the signal. The filter (5) for the selected f_0 and non-zero f_c is a narrow-band filter. The time-window (4) of $\sim$40 year length corresponds to it. Filtered AAM data thus undergo edge effect. This forces us to remove 20 years of data at the beginning and the end of
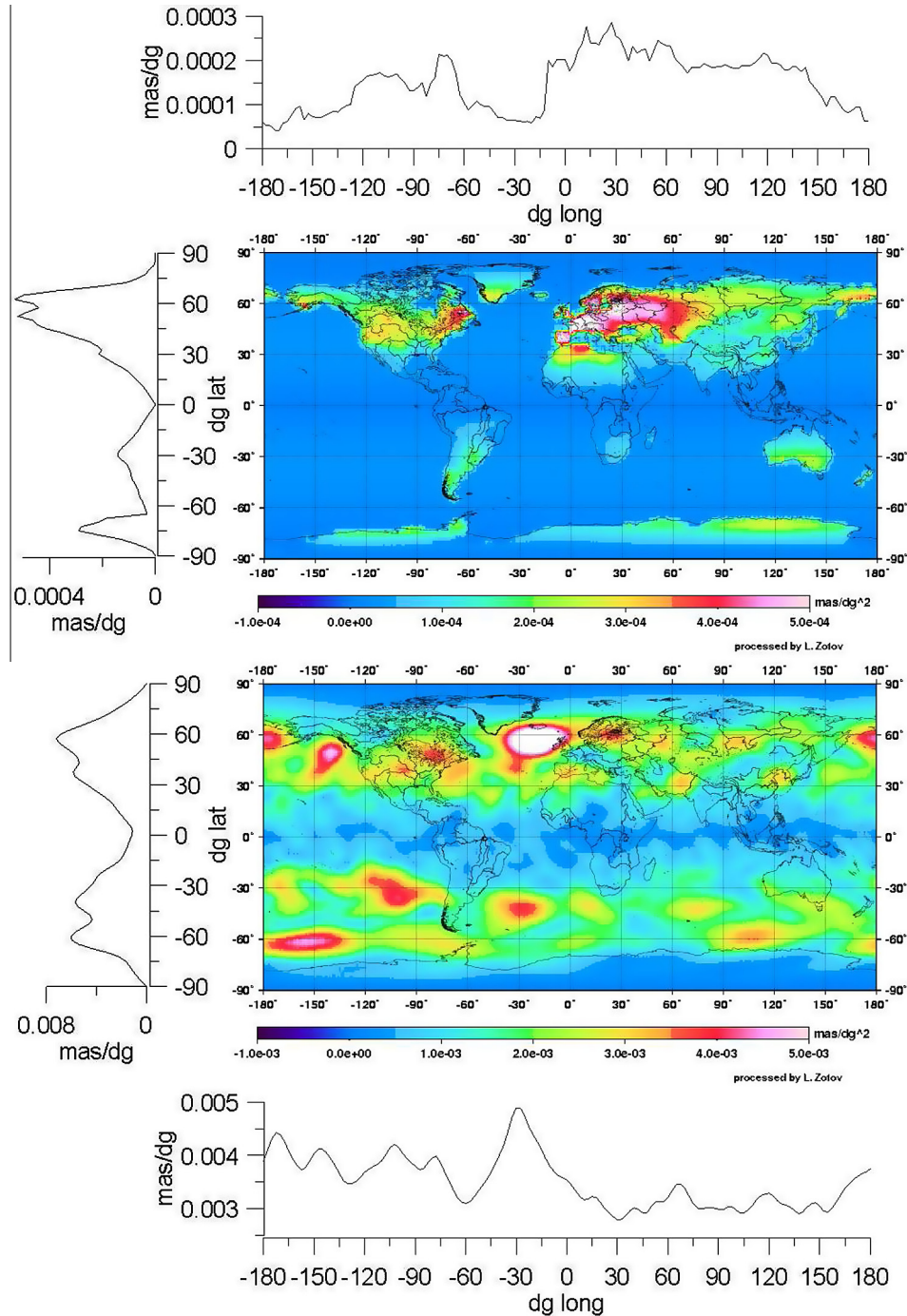
Fig. 1. The maps of the mean absolute AAM field $\langle|X|\rangle$ for pressure (left) and wind (right) in the Chandler frequency band. The plots obtained through summation over latitudes and longitudes are also shown.

the interval from the consideration. Only 1968–1991 interval remains.

To demonstrate the filter properties, in Fig. 2 we present its frequency response (5) (left), Chandler wobble (middle), and geodetic excitation (right) obtained with this filter from IERS EOP C01 PM data by methodology explained in Zotov and Bizouard (2012). The results for two values of parameter $f_0 = 1/25 \text{ yr}^{-1}$ and $f_0 = 1/70 \text{ yr}^{-1}$ are presented. The filter allows only Chandler frequency to pass,

and suppress the low-frequencies, trend, annual, and higher frequencies. The results do not change, if annual cycle is preliminarily extracted, but depend on the filter width. The Chandler wobble obtained with $f_0 = 0.04 \text{ yr}^{-1}$ (Fig. 2, top) has conventional shape, all the Chandler mode with its side-lobes passes through this filter, thus, it is chosen in this paper. The excitation for this case has quasi 20-year amplitude modulation. The signal, obtained with too much narrow $f_0 = 0.014 \text{ yr}^{-1}$ filter (bottom), has
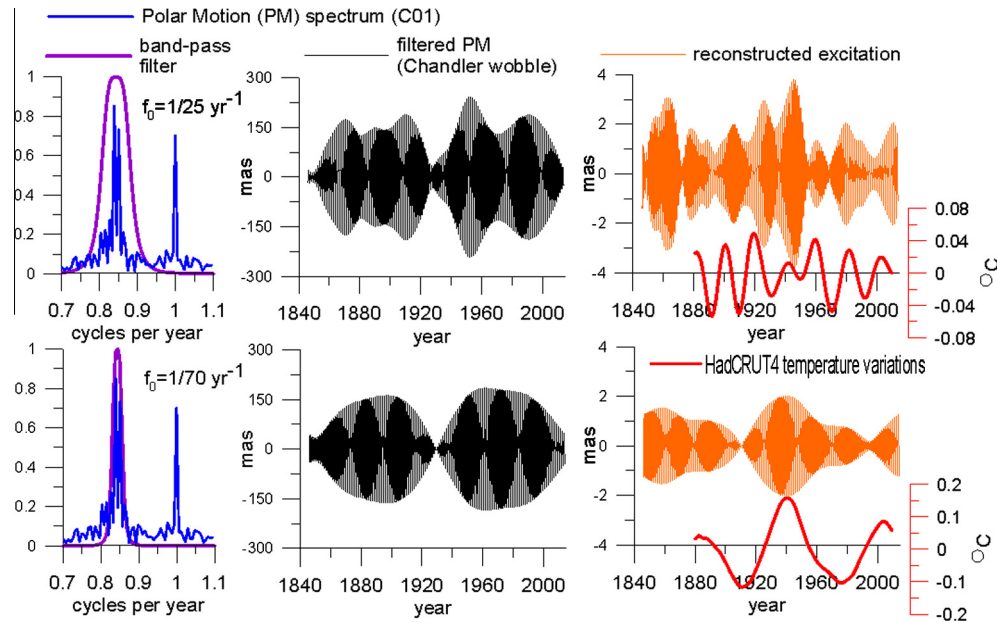
Fig. 2. Panteleev's filter frequency response superimposed on the polar motion spectrum (left), Chandler wobble (middle), and geodetic excitation (right) for two values of parameter f_0. x-components are presented, y-components are similar in shape, but shifted by $\pi/2$ (109 days). The components extracted from global Earth temperature (HadCRUT4) variability are given along the abscissa in red colour (right). (For interpretation of the references to colour in this figure legend, the reader is referred to the web version of this article.)

quasi-70-year modulation with decay in 1840s, 1930s, and 2010s. It is hidden in the signal, obtained with wider $f_0 = 0.04$ filter. Both 20 and 70-year modulations of the Chandler excitation are very similar to the natural climate variations found in the global Earth temperature and sea level (Schlesinger, 1994; Zotov, 2013), but analysis of this subject could lead us out of the scope of this paper.

Some preliminary data processing was used for AAM fields to reduce the computation time. The chosen parameters of the filter (5) permit to remove low and high-frequency part of the signal before processing, not introducing any distortions into the result. We removed the mean over 1948–2012 interval, smoothed the time series, and enlarged the temporal sampling. Low-frequency smoothing was made by Panteleev's filter (4) transformed to the low-frequency filter by centring it at zero frequency $f_c = 0$. The cut-off parameter value $f_0 = 10 \text{ yr}^{-1}$ was selected for permitting the resampling by decimation with a 10-days step, which reduced the data amount by 40 times.

3. Results of processing

Obtained AAM $X(\lambda, \phi)$ is a complex field, containing real and imaginary parts. As it was mentioned above, real part corresponds to the TRF x-coordinate axis lying in the Greenwich meridian plane and is therefore mostly influenced by zonal wind[2] and pressure changes taking place over the great Greenwich circle, encompassing both eastern Atlantic ocean and central Pacific. The imaginary

component, corresponding to the equatorial y axis in the direction 90° east, is dominated by the atmospheric changes over Asia, Indian ocean, North America and Western Southern Pacific. We will not consider separately x and y components, but will study the amplitude $|X|$ of the regional Chandler excitation. Both large positive and negative input give large module. The filter (4) extracts only the resonant prograde Chandler component, so the retrograde component does not appear in the result.

The maps of the averaged over 1968–1991 AAM module $\langle |X| \rangle$ in the Chandler frequency band for the wind and pressure terms are represented in Fig. 1. The curves, obtained through integration over meridians and parallels, are also given. The pressure input is concentrated on the continents (it is compensated over ocean by its level change is reason of the IB-hypothesis), while the wind input is stronger over the ocean. There are more continents in the Northern hemisphere, so the pressure term influence is stronger there. In the Southern hemisphere most of the pressure input comes from the coast of Antarctica. Both pressure and wind AAM input are concentrated in the temperate latitudes band $[30°, 60°]$ and $[-30°, -60°]$. This could result from larger atmospheric variability at this latitudes observed already in the initial AAM maps before filtering. For the pressure component it comes from the maxima of $\sin \phi \cos^2 \phi$ term in Eq. (3), for the wind term due to strong westerly zonal winds and atmospheric currents concentrated there (Peixoto and Oort, 1984). It is interesting to see that the average of the pressure component filed is especially large over Europe. Some pressure influence also comes from North America and Australia, which agrees with the results obtained from correlation

---

[2] Meridional wind changes at Greenwich circle influence y-component.
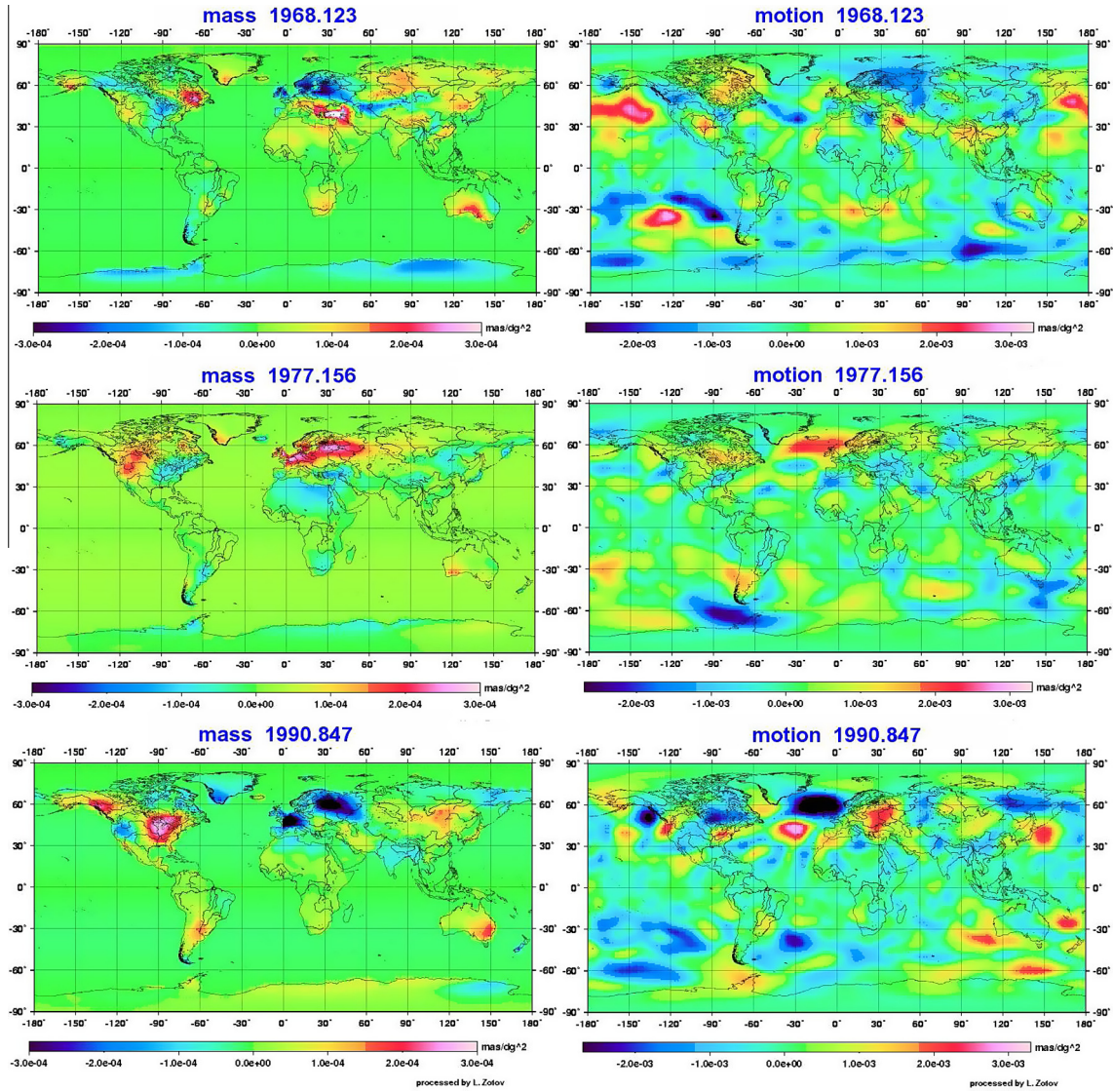
Fig. 3. Module variation $\Delta|X|$ with respect to the mean for pressure term (left) and wind term (right) in the Chandler frequency band.
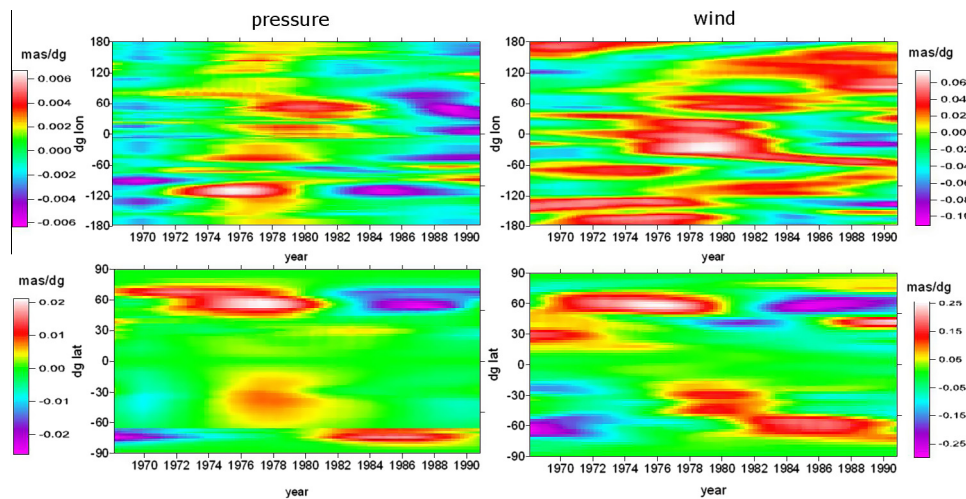
Fig. 4. Longitude-time (top) and latitude-time (bottom) Hovmoeller plots for the module offset $\Delta|X|$ with respect to the mean in the Chandler frequency band: pressure term (left) and wind term (right). Pressure input mostly comes from the continents.
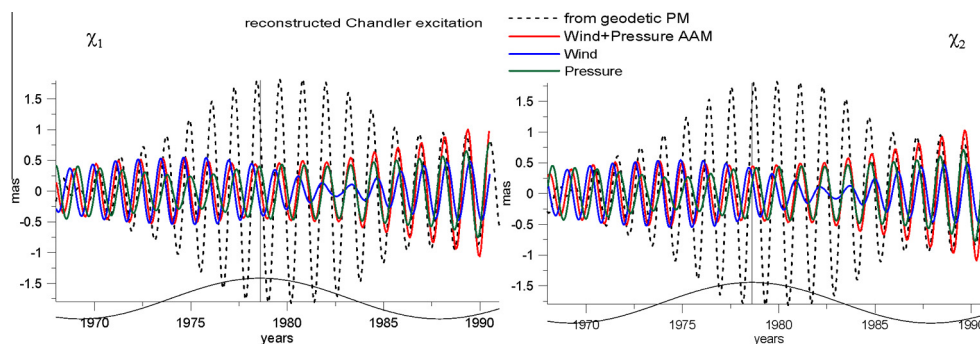
Fig. 5. Integrated EAAM χ for winds (blue line), pressure (green line), and their sum (red line) in the Chandler frequency band compared to the Chandler geodetic excitation (dashed black line) reconstructed from PM observations. 18.6-year Lunar tidal wave is given along x-axis. (For interpretation of the references to colour in this figure legend, the reader is referred to the web version of this article.)

maps in Nastula et al. (2014). The difference is in absence of large input from Asia, which could be in consequence of different analysis strategy used in our study and in Nastula et al. (2014) (we do not preliminary subtract wind input and do not correlate with integrated EAAM). For the wind term a significant maximum can be distinguished in the Northern Atlantic at the south-east from Greenland, where the Island minimum (zone of minimum pressure) is located. That is probably connected to the storms, strong winds, and pressure variations in this region, also influenced by the Gulfstream and Atlantic Multidecadal Oscillation (Schlesinger, 1994).

Fig. 3 displays three maps of the AAM module offsets with respect to the mean $\Delta|X| = |X| - \langle|X|\rangle$ in the Chandler frequency band for each of the term (pressure and wind) in 1968, 1977, and 1990 yr. The full animated set of maps is accessible as the electronic attachment to this article and at http://lnfm1.sai.msu.ru/~tempus/science/Chandler/. The time span is not long enough for a sound conclusion, but it is possible to find a repetitive pattern of ∼20-yr period. Some regions of maxima becomes minima and go back to maxima during this time interval.

We integrated AAM module offsets $\Delta|X|$ over latitudes and longitudes separately for every sampling time, and presented them on the Hovmoeller plots, Fig. 4. They reflect modulation of the Chandler excitation amplitude in particular latitude and longitude belts.

The longitude-time plot (top) for pressure (left) presents mostly horizontal patterns, where we see minima at the beginning of the time interval, maxima around 1970, and minima at the end. The maximum pattern (red) of the wind term (right) seems to spread along the diagonal. This could mean that the regions of wind influence migrates around the globe to the east in ∼20 years. In addition to complicated longitudinal migration, the north/south asymmetry is observed.

From the latitude-time plots (bottom) for both wind and pressure it is seen that maxima migrates from the Northern hemisphere to the Southern hemisphere. The maximum in 1976 at +60° becomes the minimum in 1988 yr, vice versa at −60° latitude. The animated maps also show regions of coupled behaviour. For example, maximum in the wind term over Iceland is accompanied by the minima in the Drake Passage, since they reverse their sign simultaneously. Possible some quasi-20 year variability is inherent to the wind and pressure regional AAM in Chandler band.

Speaking about the phase of atmospheric Chandler excitation, it also can be plotted on the map, but we do not present such plots because of their complex structure. The phase patterns rotates around the Earth with the Chandler period.

Finally, filtered AAM fields were integrated. The obtained total pressure and wind terms, and their sum are displayed in Fig. 5. These quantities can be compared to the Chandler geodetic excitation obtained from the PM observations, Fig. 2, top (Zotov and Bizouard, 2012). Tough it is seen from the maps in Figs. 1 and 3 that the wind input is one order of magnitude higher than the pressure input, the amplitudes of the integrated quantities are similar in size, because the winds input in the Northern hemisphere is compensated by the winds of the Southern hemisphere (Nastula and Salstein, 2012). The mean amplitudes of excitation are: 0.39 ms of arc (mas) for winds, 0.48 mas for pressure, 0.61 mas for their sum, 1.14 mas for the excitation reconstructed from observations. The phases of all the signals are quite close.

The total atmospheric input explains only ∼50% of the Chandler excitation. EAAM does not show amplitude maximum around 1979, which is observed in the excitation reconstructed from PM observations. This modulation is probably produced by the ocean input and, as shown in Zotov (2010) and Zotov and Bizouard (2012), could be related to the 18.6-year cycle of the Lunar tide (Chapman and Lindzen, 1970).

4. Conclusion

By applying the Panteleev filtering technique, we derived the maps of regional atmospheric input to Chandler wobble excitation for pressure and wind terms. For pressure term the input comes from the continents, mostly from the Northern hemisphere, especially Europe. For winds,

the Chandler excitation mostly results from the oceans area, especially North Atlantic. In Hovmoeller plots we discovered anti-correlated pattern of the atmospheric Chandler excitation in the Northern and Southern hemispheres evolving with a quasi-period of ∼20 years. When the AAM fields are integrated, this wave disappears in Chandler excitation amplitude. The total EAAM is compared to the corresponding geodetic excitation, deduced from PM by Eq. (1) inversion completed by Panteleev's filtering. Whereas the atmospheric input accounts for about 50% of excitation, it does not show the ∼20 year amplitude modulation of the Chandler excitation, found in earlier work (Zotov and Bizouard, 2012) and probably related to the 18.6 year Moon orbital precession. For investigating this problem, our study has to be extended to the oceanic excitation.

Acknowledgements

Appendix A. Supplementary data

Supplementary data associated with this article can be found, in the online version, at http://dx.doi.org/10.1016/j.asr.2014.12.013.

References

Bizouard, C., Remus, F., Lambert, S., et al., 2011. The Earth's variable Chandler wobble. Astron. Astrophys. 526 (A106).

Brzezinski, A., Nastula, J., 2002. Oceanic excitation of the Chandler wobble. Adv. Space Res. 30 (2), 381–386.

Brzezinski, A., Bizouard, Ch., Petrov, S., 2002. Influence of the atmosphere on earth rotation: What new can be learned from the recent atmospheric angular momentum estimates? Surv. Geophys. 23 (1), 33–69.

Brzezinski, A., Dobslaw, H., Dill, R., et al., 2012. Geophysical excitation of the Chandler wobble revisited. Geod. Planet Earth Int. Ass. Geodesy Symp. 136 (3), 499–505.

Chapman, S., Lindzen, R., 1970. Atmospheric Tides: Thermal and Gravitational. Springer.

Gross, R., 2000. The excitation of the Chandler wobble. Geophys. Res. Lett. 27 (15), 2329–2332.

Gross, R., Fukumori, I., Menemenlis, D., 2003. Atmospheric and oceanic excitation of the Earth's wobble during 1980–2000. J. Geophys. Res. 108 (B8), 2370.

Lambeck, K., 1980. The Earth's Variable Rotation: Geophysical Causes and Consequences. Cambridge University Press.

Liao, D.C., Zhou, Y.H., Liao, X.H., 2007. Comparison of wind contributions to Chandler wobble excitation. Chin. Astron. Astrophys. 31, 57–65.

Munk, W., MacDonald, G., 1960. The Rotation of the Earth. Cambridge Univ. Press.

Nastula, J., Salstein, D.A., 2012. Regional geophysical excitation functions of polar motion over land areas. Geod. Planet Earth IAG Symp. 136 (3), 499–505.

Nastula, J., Ponte, R.M., Salstein, D.A., 2007. Comparison of polar motion excitation series derived from GRACE and from analyses of geophysical fluids. Geophys. Res. Lett. 34 (L11306).

Nastula, J., Salstein, D., Kolaczek, B., 2009. Patterns of atmospheric excitation functions of polar motion from high-resolution regional sectors. J. Geophys. Res. 114, B04407.

Nastula, J., Gross, R., Salstein, D.A., 2012. Oceanic excitation of polar motion: identification of specific oceanic areas important for polar motion excitation. J. Geodyn. 62, 16–23.

Nastula, J., Salstein, D., Gross, R., 2014. Regional multi-fluid-based geophysical excitation of polar motion. In: Proceedings of IAG General Assembly 2011. Springer, pp. 467–472.

Panteleev, V.L., Chesnokova, T.S., 2011. Problem deconvolution in inertial gravimetry. Moscow Univ. Phys. Bull. 66 (1), 78–82.

Peixoto, J.P., Oort, A.H., 1984. Physics of climate. Rev. Mod. Phys. 56 (3), 365–429.

Salstein, D., 2000. Atmospheric excitation of polar motion. ASP Conf. Ser. 208, 437–446.

Schlesinger, M.E., 1994. An oscillation in the global climate system of period 65–70 years. Nature 367 (6465), 723–726.

Sidorenkov, N.S., 2009. The Interaction Between Earth's Rotation and Geophysical Processes. Wiley-VCH Verlag, Weinheim.

Zhong, M., Yan, H., Zhu, Y., 2002. The investigation of atmospheric angular momentum as a contributor to polar wobble and length of day change with AMIP II GCM data. Adv. Atmos. Sci. 19 (2), 287–296.

Zhou, Y.H., Salstein, D.A., Chen, J.L., 2006. Revised atmospheric excitation function series related to Earth's variable rotation under consideration of surface topography. J. Geophys. Res. 111, D12108.

Zotov, L.V., 2010. Dynamical modeling and excitation reconstruction as fundamental of Earth rotation prediction. Artif. Satell. 45 (2), 95–106.

Zotov, L.V., 2013. Sea level and global earth temperature changes have common oscillations. Odessa Astron. Publ. 26 (2), 289–291.

Zotov, L.V., Bizouard, C., 2012. On modulations of the Chandler wobble excitation. J. Geodyn. 62, 30–34.

Zotov, L.V., Panteleev, V.L., 2012. Filtering and inverse problems solving. In: Wang, Y.F., Yagola, A.G., Yang, C.C. (Eds.), Computational Methods for Applied Inverse Problems, pp. 169–194.